ADVANCED PHOTONICS RESEARCH Open Access
www.adpr-journal.com

Nanosecond-Pulsed Laser Beam Shaping with a Liquid Crystal Spatial Light Modulator for Rapid Microtexturing of Metallic Surfaces

Juan I. Ahuir-Torres, Pasquale Franciosa, Tahsin T. Öpöz, Martin C. Sharp, Musa B. Bashir, and Hiren R. Kotadia*

Laser surface texturing can improve the functional properties of metallic materials, with the texture shape being a crucial factor. The spatial light modulator (SLM) is used to design the shape of individual textures. However, generating deep microtextures with precise shapes on metallic materials currently requires extended processing times, limiting their use in industrial applications. This study investigates the generation of the microtexturing patterns with various shapes on stainless steel 316 L surface using a SLM. The method combining computer-generated holograms with images demonstrates high energy fluence efficiency. The holograms determine the reconstruction distance, shape, and size of the textures. Patterns of the textures with various complex shapes (e.g., circular, triangle, square, hexagon, and other), 6–12 µm depth and 50–70 µm width are achieved using only 5 pulses (200 µs per texture) and 25 kHz pulse frequency rate. This method achieves texturing of 10 × 10 mm areas with various shapes in just 2 s, offering a processing speed ≈500 times faster than current state-of-the-art ultrashort laser pulse techniques, significantly advancing the efficiency of microtexturing processes.

1. Introduction

Surface texturing is a method used to functionalize the surfaces, imparting new properties to the material such as enhanced adhesion,[1] lubricant reservoir,[2] corrosion resistance,[3] biocompatibility,[4,5] antibacterial and antimicrobial,[4] and plasma resonance.[6] Laser surface texturing (LST) is the most widely utilized technique due to its high precision, automation, nonwearing tool, environmental friendliness, and reproducibility. LST techniques have been successfully employed in the functionalization of various materials, including metals, ceramics, polymers, and biological tissues.[7–9] For these reasons, LST is utilized in various industries such as structural, automotive, biomedical, maritime, power, aerospace, and electronic.[7,8,10] The degree and type of surface functionalization is defined by the texture density of the patterns, shape, and size of the texture.[3,10] In traditional LST, textures are typically limited to simple circular or square shapes and are constrained to sizes in the order of hundreds of micrometers. This limitation reduces the ability to tailor surface functionality for applications requiring more intricate, microscale designs to enhance specific properties like hydrophobicity, adhesion, or friction. Laser beam shaping (LBS) offers a solution by enabling precise control over the laser beam's shape and intensity profile, allowing the creation of diverse, complex textures at a microscale level, which can significantly enhance surface functionalisation potential.[11–13]

LBS enables precise design of the laser beam by redistributing its irradiation and phase. LBS techniques are typically categorized into three approaches: aperture, field mapping, and beam integration.[12,14] Among these, beam integration is the most widely used due to its high laser energy efficiency, making it ideal for industrial applications that require efficient, high-quality texturing. The beam integration technique is typically implemented using a spatial light modulator (SLM), which can be either optical or electrical. In optical SLM, LBS is achieved by projecting light encoded with an image onto the front and back surfaces of materials. In contrast, electrical SLM generates and modifies images by applying voltage to electrodes (pixels). The electrical SLM offers higher accuracy compared to the optical method and can be implemented with various technologies, such as liquid crystal, magneto-optic, deformable mirrors, and acousto-optic devices.[15] Among these, the liquid crystal (LC) SLM is particularly notable for its flexibility,

J. I. Ahuir-Torres, T. T. Öpöz, M. C. Sharp, H. R. Kotadia
School of Engineering
Liverpool John Moores University
Liverpool L3 3AF, UK
E-mail: j.i.ahuirtorres@ljmu.ac.uk

P. Franciosa, H. R. Kotadia
WMG
University of Warwick
Coventry CV4 7AL, UK

M. B. Bashir
Civil and Environmental Engineering
University of Liverpool
Liverpool L69 7ZX, UK

The ORCID identification number(s) for the author(s) of this article can be found under https://doi.org/10.1002/adpr.202500090.

DOI: 10.1002/adpr.202500090

high pixel count, and ease of programming.[16] These advantages have led to its extensive use in LBS applications with ultrashort (ps and fs) pulsed lasers.

In 2015, Kuang et al.[11] shaped the laser beam by the application of a mask in LC-SLM. The 1064 nm 20 ps pulsed laser was used to texture stainless steel 316 L (316 L). The application of the mask, however, reduced the energy efficiency of the laser beam for achieving a well-defined footprint. Chen et al.[13] investigated the design of the hierarchical micro/nano microstructure on 316 L using a LC-SLM and iris. An 800 nm 120 fs pulsed laser was used to texture the metallic alloys. They successfully produced footprints on 316 L with diverse shapes such as triangle, square, pentagon, and hexagon by utilizing a mask. The footprints also exhibited internal groove and laser-induced periodic surface structures (LIPSS) that can be set using an iris. The researchers generated the footprints (shallow texture) on metallic alloy with femtosecond pulsed laser in 5 s (5000 pulses), which is an excessive time for industrial applications. In 2016, Li et al.[17] successfully created square and circle dimples with the flat laser-beam profile. They applied a mask in grayscale on a LC-SLM to produce a flat laser-beam profile with various shapes. The grayscale enabled generation of the flat profile, but it caused a reduction in the laser energy. A 20 ps 1064 nm laser was employed to create the dimples between 3 μm (flat beam) and 9 μm (Gaussian beam) with 1 s production time. Two years later, Liu et al.[18] enhanced the texture shapes initially generated by Kuang et al.[11] through combining two holograms. The investigators integrated the masks with grating period hologram to produce footprints with high-quality shape in just 0.5 s. The grating period improved the quality of the texture shape. The pulsed laser operated at 100 fs and 800 nm. Recently, Fang et al.[19] successfully increased the shaped laser-beam ablation through multiburst generation. A LC-SLM was employed to produce these bursts with a 10 ps 1064 nm pulsed laser. The multibursts mitigated the effect of the plasma on the subsequent laser pulses, reducing the energy of the laser pulses required.

LC-SLM has also been utilized in short (ns) pulsed lasers in the literature,[16,20,21] though less comprehensively. In 2010, Beck et al.[16] designed the beam of the green (532 nm) 65 ns pulsed laser with LC-SLM. The inverse Fourier transform algorithm was employed to produce the holograms. The researchers successfully generated textures with dimensions in hundreds of micrometers with diverse shapes (i.e., circle, square, triangle, and ring) on glass and polyimide coating. The texture processing took 100 and 3.2 ms for glass and polyimide coating, respectively. Kaakkunen et al.[20] used LC-SLM to inscribe patterns on 316 L using two 1064 nm short pulsed (110 and 1500 ns). The alphabet letters were formed of various shots, and the process took 450 μs. In 2020, Dupuy et al.[21] generated square footprints on 316 L using a 1064 nm, 100 ns pulsed laser on LC-SLM. The laser beam was also reshaped to achieve a flat profile of the laser beam. They moreover produced laser-induced periodic surface structures with a 1030 nm, 500 fs pulsed laser in conjunction with LC-SLM.

Furthermore, LBS with LC-SLM for texturing applications has been extensively studied in the literature, with most research focused on ultrashort pulsed lasers. Processing times for these textures typically range from 0.5 to 5 s, achieving a maximum depth of only 9 μm with 1 s of laser irradiation per texture.[13,17,18] These limitations restrict the application of this technology in real-world settings, as they hinder the efficient texturing of large areas within a practical timeframe. Nanosecond pulsed lasers offer a promising alternative to ultrashort pulsed lasers, as they are commercially available and provide higher energy outputs. Current studies on the use of LC-SLM with nanosecond pulsed lasers, however, have shown limitations, often producing shallow textures with areas in the hundreds of micrometers or requiring multiple shots to achieve the desired depth (from 1 to 9 μm) and shape. These factors complicate the application of this technology in the field of texturing. Therefore, a detailed study is required to fully explore the potential of combining LC-SLM with nanosecond pulsed lasers. Such research could address existing limitations related to shape precision, depth control, and processing time. Overcoming these challenges would significantly enhance the applicability of this technology in industrial surface treatment applications, enabling more efficient and versatile texturing methods.

For that reason, the current study investigates the use of LC-SLM to generate deep microtextures with different shapes, namely circles, triangles, squares, and hexagons on 316 L stainless steel. This approach utilizes an infrared (1064 nm) nanosecond pulsed (200 ns) laser in combination with holograms created through images generated in PowerPoint software and the computer-generated hologram (CGH) method.[22] The texture quality was evaluated with an optical light profilometry and scanning electron microscopy (SEM). Dimples with various shapes (e.g., circular, ellipsoid, triangular, square, pentagonal, hexagonal, tangent cone, and droplet), width of ≈50 μm, and depths ranging from 6 to 12 μm were successfully generated on 316 L with only 5 pulses with this novel method. This approach enables texturing of large surfaces (10 × 10 mm) in just 2 s, which is ≈500 times faster than the previously reported study.[19] This innovative method demonstrated the potential industrial applications of this technology.

2. Experimental Section

2.1. Materials

For the texturing experiment, 316 L stainless steel, supplied by Columbus Stainless Ltd, was used. Its chemical composition, shown in **Table 1**, was chosen for its excellent corrosion resistance, mechanical properties, and widespread application in various industries.

Before the texturing experiment, the samples were polished using abrasive SiC paper with a P1200 grit to achieve a surface roughness (Sa) of 120 nm, which was considered optimal for texturing.[23]

2.2. Laser Experiment Set-up and Procedure

The laser system consisted of an infrared (IR) pulsed fiber laser, an optical system, and a three-axes automatic table (**Figure 1**).

Table 1. 316 L chemical composition in weight percent (wt%).

Element	Fe	C	Cr	Cu	Mn	Mo	Ni
(%) wt.	Bal	0.025	16.200	0.120	1.660	2.057	10.070

ADVANCED PHOTONICS RESEARCH Open Access
www.adpr-journal.com

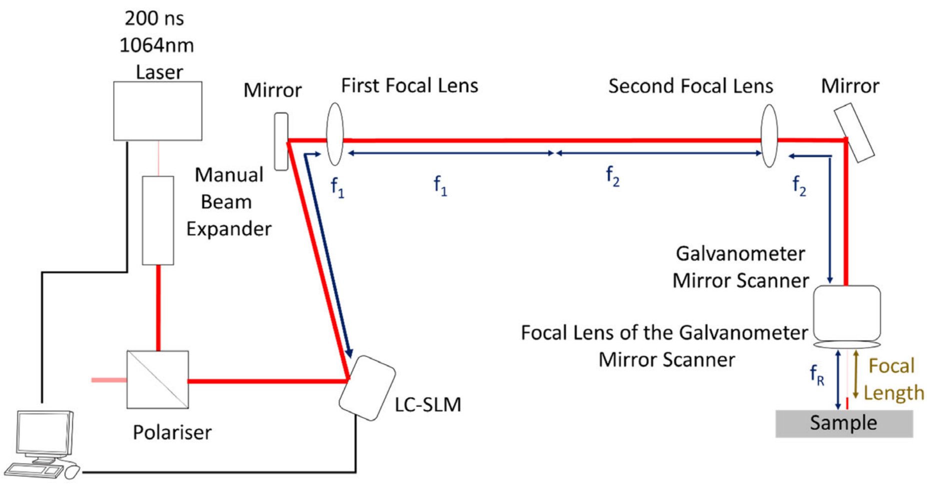

Figure 1. Schematic drawing of the optical system. f_1 is the focal length of the first focal lens, f_2 is the focal length of the second focal lens, and f_R is the image reconstruction length.

The IR fiber pulsed laser model was a SPI Laser (UK) G3 20 W nanosecond pulsed fiber laser. The laser exhibited a wavelength of 1064 ± 5 nm, and a near TEM_{00} mode with beam quality factor $M^2 = 2.1$. The laser can work with pulse lengths varying from 9 to 200 ns, and pulse repetition frequencies ranging from 1 to 500 kHz. The maximum average power of the laser was 22 W, exhibiting a maximum pulse energy of 880 μJ before the optical system. Power and pulsed energy were measured with an Ophir laser power meter system using a 30A-N-SH ROHS head and Nova II display software.

The optical system comprised a manual 1064 nm beam expander (Linos (Qioptiq) 2-8×, Thorlab), polarizing beam splitter cube 700–1300 nm (PBS205, Thorlab), LC-SLM (Pluto 2, Holoeye), silver mirrors (PF10-03-P01, Thorlab), two plano-convex focal lenses (LA1908-C-ML N-BK7, Thorlab), and a galvanometer mirror scanner (Nutfield Extreme-15-YAG). The manual 1064 nm beam expander expanded the laser beam to a diameter of 5.77 mm. The laser irradiation was subsequently polarized with the polarizing beam splitter cube and directed to LC-SLM, which was employed to shape the laser beam. The polarization of the laser irradiation was 0°, and the laser beam was incident on LC-SLM with ≤10° to minimize the laser power reduction.[11,24,25] Multiple silver mirrors were used to guide the laser beam to the two plano-convex focal lenses, both of which had the identical focal length ($f_1 = f_2$) of 500 mm. The distance between LC-SLM and the first plano-convex focal lens was also equal to the distance from the second plano-convex focal lens to galvanometer mirror scanner. This arrangement, combining LC-SLM, the plano-convex focal lenses, and a galvanometer mirror scanner, formed a four-lens system, enabling image transport over long distances.[16,18,22,24–26] The galvanometer mirror scanner was equipped with a f-theta focusing lens of 100 mm focal length. The samples were placed on the 3-axes automatic table, which was used to precisely adjust the distance from the galvanometer mirror scanner to the sample surface. The LC-SLM had a resolution of 1920 pixels × 1080 pixels with 8 μm pixel size. Holoeye Pluto 2.1 Configuration Manager software was employed to configure the LC-SLM parameters, while CGH was carried out with Holoeye SLM Pattern Generator 5.2 software. The galvanometer mirror scanner was also used to displace the laser beam on the samples with velocities ranging from 0.1 to 5000 mm s^{-1}.

It is noted that the laser-beam power was reduced to 33% of the laser power upon reaching the samples due to combined effect of the polarizer, mirrors, focal lenses, and galvanometer mirror scanner. The most significant power lost was produced by polarizer, which was 50%. The mirrors, focal lenses, and galvanometer mirror scanners collectively contributed to 17% reduction of the laser power.[27]

The textures were generated using 5 pulses, each with a pulse length of 200 ns, and with the maximum pulse energy 800 μJ, resulting in effective energy of 295 μJ on the sample surface. The scan speed was set at 2500 mm s^{-1} with the galvanometer mirror scanning, and the pulse frequency rate was 25 kHz to get a distance between textures of 100 μm to avoid the overlap of the dimples (**Table 2**).

The LC-SLM worked within a voltage range from 0.98 to 4.99 V, with a phase of 2π and 162 NLUTs. The Holoeye Pluto 2.1 Configuration Manager software was employed to configure the LC-SLM parameters. Eight types of texture shapes were

Table 2. Selected laser parameters used for the texturing experiment.

Parameters	Values
Wavelength [nm]	1064
Transverse electromagnetic mode	00
Beam quality factor	2.1
Expanded laser-beam diameter [mm]	5.77
Pulse length [ns]	200
Atmosphere	Natural air
Pulse frequency rate [kHz]	25
Pulse energy [μJ]	295
Laser radiation polarization	45°
Scan speed [mm s^{-1}]	2500
Pulse number	5

created, including circle, ellipsoid, triangle, square, pentagon, hexagon, tangent cone, and droplet. The details of the holograms used to generate the texture shape are described in Section 2.1.

2.3. Surface Characterization

The topography of the textures was characterized using an optical interferometric light microscope (ContourGT optical profiler, Bruker), operating with green light and 50X magnification. The textures and texture patterns were evaluated using a scanning electron microscope (TM4000 Plus Tabletop SEM series, Hitachi), working with secondary electrons, 15 kV potential acceleration, 70 μA current tension, and 2 μm spot size.

3. Results

3.1. Hologram Generation

The generation of a high-quality hologram was a crucial factor in achieving accurate LBS, which can produce microtexture with depth. The holograms were influenced by various parameters (e.g., original image, image scale factor, the focal length of the superimposed Fresnel zone lens, maximum unit cell size, and gray scale).

The original black-and-white images generated using PowerPoint exhibited the best results, with a geometry of the laser beam represented by the white and the background by the black area (**Figure 2**). The use of the colors or gray scale diminished the quality of the LBS. The size ratio between white and black areas was 0.1; larger ratios decreased the energy fluence of the laser radiation, whilst lower ratios reduced the quality of the texture. It is noteworthy that the images had to be bitmap format of a resolution of ≥600 DPI, as a lower resolution reduces the quality of the LBS.

The minimum image scale factor, 0.01, produced textures with good quality for the ellipsoid, triangular, tangent cone, and droplet shape. In the case of the textures with circular, square, pentagon, and hexagon geometries, the most suitable image scale factor was 0.02. Although the lowest image scale factor generated the highest energy fluence, some shapes exhibited a reduction in the quality of the texture. The size of the texture in the reconstruction image length was also defined by the image scale factor. The suitable minimum image scale factor is significantly influenced by the geometry type. The elongated morphologies (i.e., ellipsoid, triangle, tangent cone, and droplet) exhibit lower image scale factor compared to proportional shapes (i.e., circle, square, pentagon, and hexagon). The low image scale factor can cause elongation effects, which are mitigated in elongated shapes.

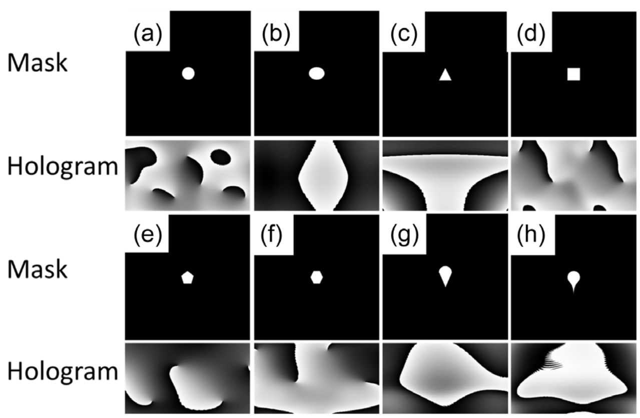

Figure 2. Mask and holograms of the a) circle, b) ellipsoid, c) triangle, d) square, e) pentagon, f) hexagon, g) tangent cone, and h) droplet texture on 316 L surface.

The Fresnel zone lens was set to 0.001 to minimize the energy lost during the addressing of the laser beam to sample. Although a higher Fresnel zone lens can increase the energy fluence with high-quality, it can also produce undesired laser dispersion before reaching the sample, resulting in the reduction of the laser energy fluence. Thus, the superimposed Fresnel focal length (f_F) is defined by Equation (1),[25] measured 14 511 mm

$$f_{\mathrm{F}} = \frac{\mathrm{LC-SLM\ width\ (in\ pixel)} \times \mathrm{Pixel\ size}}{\mathrm{Wavelength} \times \mathrm{Fresnel\ zone\ lens}} \tag{1}$$

it is noted that the reconstruction image length (f_R), the distance from the last focal length (galvanometer mirror scanner focal length), is determined by f_F, as indicated the Equation (2),[25] being 99.2 mm

$$f_{\mathrm{R}} = f_{\mathrm{L}} - \left[f_{\mathrm{L}} \times \left(\frac{f_{\mathrm{F}} - D_{\mathrm{LC-SLM}}}{f_{\mathrm{F}} + f_{\mathrm{L}} - D_{\mathrm{LC-SLM}}} - 1 \right) \right] \tag{2}$$

where, f_L is the focal length of the galvanometer mirror scanner lens, and $D_{LC\text{-}SLM}$ is the distance from LC-SLM to the galvanometer mirror scanner focal lens.

The low maximum unit cell size (96 pixels) resulted in texture morphologies consisting of the multishots, while the high maximum unit cell (1080 pixels) size produced the geometries formed with only one shot. The concept of maximum unit cell is analogous to the resolution of an image, when the lower resolution corresponds to the larger pixel size of the image. Thus, the generation of the textures at micro scale requires high maximum unit cell, such as 1080 pixels.

The pulse energy after LC-SLM was observed to be the lowest (50 μJ) at a grayscale value of 0 and 255, while the highest pulse energy (400 μJ) was achieved at a grayscale value of 125. The reflectivity of the liquid-crystal section determines the laser energy after LC-SLM, which is defined by the grayscale of the hologram. The influence of the grayscale on the laser energy is typically sinusoidal, but some variation can be observed according to the laser polarization.[11,24,28] To achieve highest laser energy efficiency, the grayscale value corresponding to the maximum efficiency (400 μJ) was used.

3.2. LBS on Textures

The textures at 5 pulses and 290 μJ designed using the holograms applied on LC-SLM exhibited the desired shape (**Figure 3**). All textures presented displayed material outside of the textured area, which is attributed to the explosion of the liquid–gas bubble. At high energy fluence, the nanosecond pulsed laser generates a gas bubble around the liquid material. When the pressure of the gas on the liquid material is high, the bubble bursts, causing

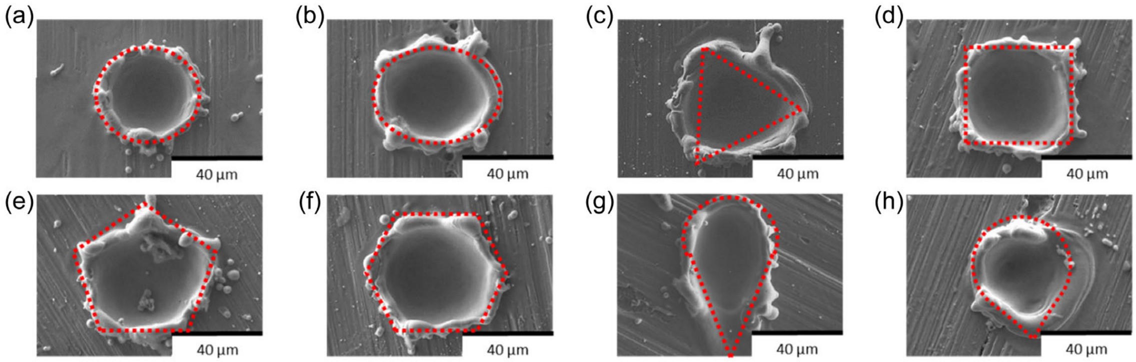

Figure 3. SE-SEM pictures of the textures with a) circle, b) ellipsoid, c) triangle, d) square, e) pentagon, f) hexagon, g) tangent cone, and h) droplet shape on 316 L.

the ejection of the melted material outside of the textured zone.[29,30] A crest was observed around the texture due to the accumulation of the melted material within the textured zone rim. The gas pressure exerted on the molten material displaces it toward the rim of the laser-impacted zone.[9,23] The hydrodynamic expansion also contributes to the molten material amassing on the textured zone rims.[29] After the laser impact, the molten material quickly re-solidifies due to the heat dissipation of the liquid into the bulk material.[9,23] Both phenomena indicate that the ablation mechanism is explosion phase.[30]

This ablation mechanism resulted in the swelling of certain textures (Figure 3c and d). The hydrodynamic expansion and the gas pressure provoke outward movement of molten material beyond the laser-treated zone, leading to imperfect formation of the texture shape. The crest of the textures exhibited various imperfections, including fractures and cracks. The bubble explosions generated by the subsequent pulses produce stress on the crest generated by previous pulses. These stresses contribute to the crack formation on the crest, which can potentially lead to the fracture of the crest.[31] Despite this imperfection, the overall quality of the textures was good.

Most of the textures presented a cross-sectional profile with a shape similar to semicircle, which can be attributed to Gaussian profile of the laser beam (**Figure 4**a–f and h). The energy fluence of the nanosecond pulsed laser is insufficient for the Gaussian profile to completely ablate the metallic material. Only the Gaussian profile top provides sufficient energy fluence for ablating the material, resulting in a semicircular shape. It is noted that the maximum energy fluence into laser beam is at the peak of the Gaussian beam.[22,23]

The textures with tangent cone shape (Figure 4g) exhibited a different profile compared to the other textures. The profile formed of the valley with a straight wall and another with significant inclination. This profile resembled a “wedge”; hence, it is referred to “wedge” profile. The LBS on two dimensions exhibited a significant impact on the 3D energy distribution, particularly when the geometry was extremely elongated. This phenomenon will be further explored in future studies, including the potential design of the laser-beam profile.

The depth and the width of the textures varied depending on the texture geometries (**Figure 5**). Textures with ellipsoid, pentagon, hexagon, and tangent cone exhibited two distinct widths: a larger and a smaller one. This variation of the width is attributed to the elongation of the laser-beam profile, which produces textures with dual width. The textures with tangent cone shape exhibited both the maximum and minimum width, measuring 44 and 70 µm, respectively. The extreme elongation of the laser-beam profile required to generate the tangent cone shape resulted in the largest difference between widths. The textures with circle, triangle, square, and droplet geometries exhibited only single width, ranging from 50 to 60 µm. This is attributed to the good homogeneity of the laser-beam profile for this type of texture shapes.

The texture with circle shape exhibited the greatest depth, measuring 12 µm, whilst the texture with droplet shape had the shallowest depth at 6 µm. Most of the other textures showed a similar depth, ranging from 10 to 8 µm, with the exception of the texture with ellipsoid geometry, which had a depth of 7 µm. This observation suggests that the two-dimension design of the laser-beam profile influences the laser pulse intensity, resulting in the reduction of the energy for certain cases.[27,32]

The texture patterns designed using LC-SLM can be seen in **Figure 6**. The distance between textures was 100 µm, and the total textured area measured 10×10 mm. The texturing of these areas only required 2 s, resulting in the single texture generation ratio of 200 µs/texture. Although some textures exhibited some imperfections (i.e., swollen, fractures of the crests, and particles on texture), most of the textures showed a well-shaped. The inconsistency in the imperfections across the textures is attributed to the heterogeneities of the surfaces (e.g., local roughness, stain, and chemical heterogeneities). Surface pretreatment can potentially mitigate these imperfections, although achieving these conditions can be a challenge for a typical industrial environment.

4. Discussion

The generation of the dimples at microscale (µm) with various morphologies (e.g., circular, triangle, square, and tangent cone) within a short processing time (500 times shorter than the time reported in the literature)[19] was successfully achieved through the optimal hologram design. Imperfect holograms can reduce the energy fluence and compromise the shape quality, hindering the generation of the texture with the desired morphology. A

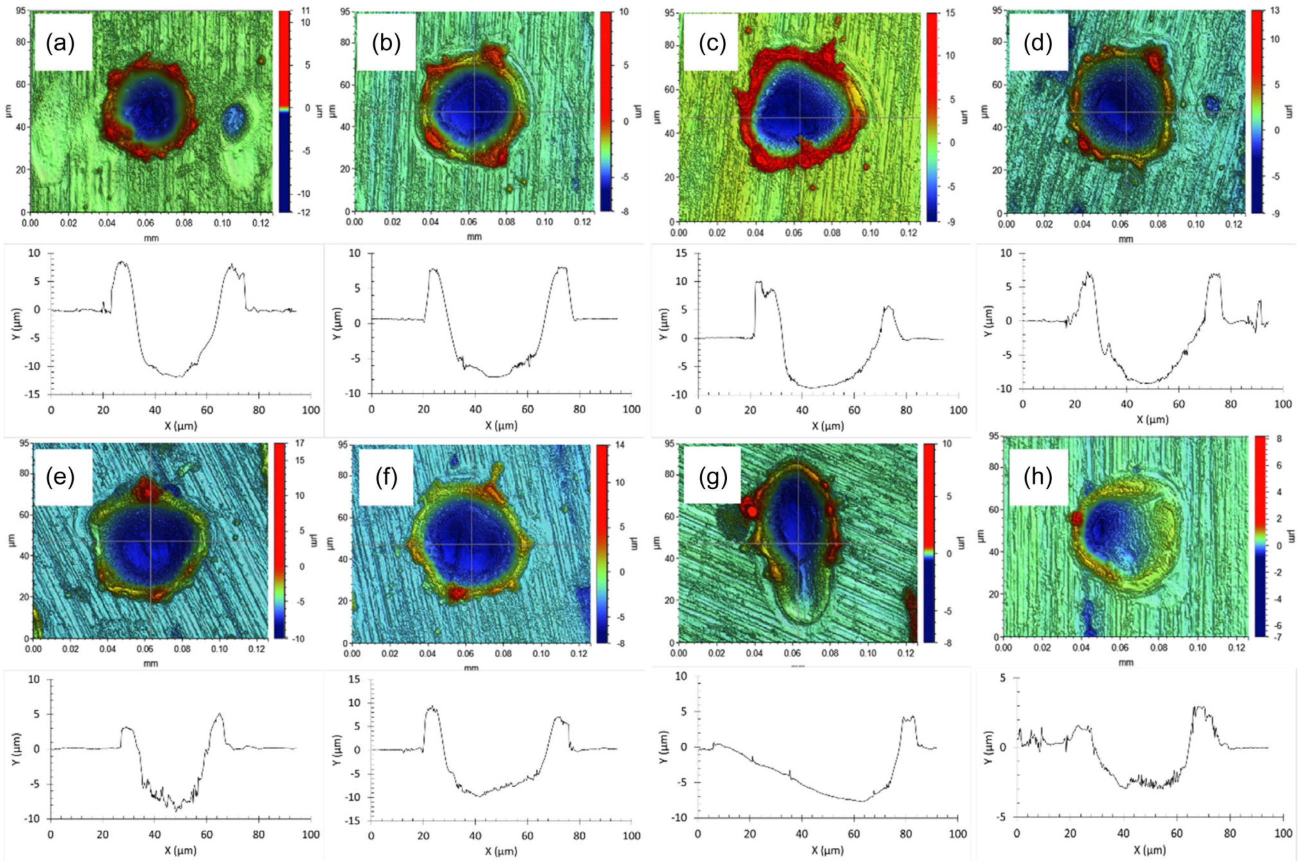

Figure 4. Profile of the textures with a) circle, b) ellipsoid, c) triangle, d) square, e) pentagon, f) hexagon, g) tangent cone, and h) droplet shape on 316 L.

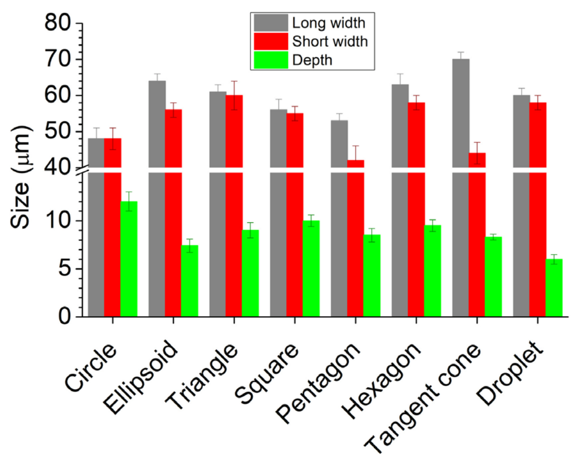

Figure 5. Depth, long, and short width of the dimples.

comprehensive understanding of the LC-SLM parameters was crucial to design the most efficient holograms. Key parameters to design the hologram using the novel method included the shape scale in the images, scale factor, quality of the images, and pixel counts.

The focused laser-beam diameter was influenced exclusively by the shape scale in the images and the scale factor due to the possibility of setting the Fresnel zone lens. This flexibility permitted precise control over the laser-beam size and shape, thus avoiding the typical inverse relation of the shaped laser-beam size with the distance from LC-SLM to the focal lens of the galvanometer mirror scanner, which is a common issue encountered with LC-SLM systems that have a fixed Fresnel zone lens. The laser-beam diameter with microscale requires long LC-SLM-focal lens distances, which typically are between 20–25 m. Excessive length can reduce the quality of the texture shape.[11,24] The ability to conveniently adjust the image reconstruction length also presents a significant advantage for LC-SLM with settable Fresnel zone lens in comparison with the classic LC-SLM.[25]

The method involving the CGH in conjugation with images exhibited less energy loss compared to the mask method. The mask method shapes the laser beam by applying a mask to the inner portion of the original laser beam. This process causes a portion of the laser beam to be filtered out, reducing the energy fluence reaching the surface. Although the mask method can generate laser beams with high-quality of shapes at reduced size (low pixel counts), this approach necessitates a large pulse number to generate a single texture, increasing the processing time.[11,24] The limitations of the mask method were absent in the approach presented in this study, as it employs the entirety of the laser beam and maintains the independence of the laser energy from the laser-beam size. It is important to note that the optimal shape of the dimples was achieved by using high pixel count (1080 pixels).

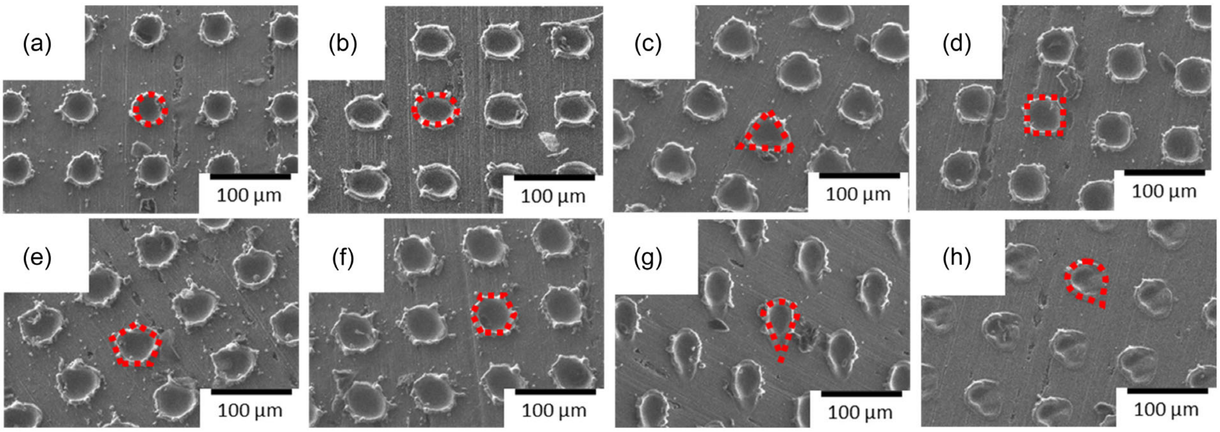

Figure 6. SE-SEM images of the patterns of textures with a) circle, b) ellipsoid, c) triangle, d) square, e) pentagon, f) hexagon, g) tangent cone, and h) droplet shape on 316 L.

These advantages enabled a method based on CGH in conjugation with images to generate a shaped laser beam at microscale with high pulse energy, resulting in laser pulses with high energy fluence. The phase explosion is the ablation mechanism for nanosecond pulsed lasers on metals at high energy fluence, characterized by higher ablation rate compared to other ablation mechanisms, such as normal evaporation.[31] The textures with significant depths (from 6 to 12 µm) on 316 L are attributed to the mechanism explosion phase. Although the phase explosion led to some imperfections in the textures (i.e., swelling, fractured, and broken crests), the overall textures exhibited good morphology. The significant depth of the textures contributed to excellent shape quality. While the employment of the ultrashort (pico and femtosecond) pulsed laser can mitigate this imperfection, the pulse number or processing time required to generate a texture is considerably longer. For instance, Kuang,[11] Li,[24] and Liu[18] reported that generating a single texture required seconds or hundreds of milliseconds. In the optical case, a texture with 9 µm depth required 1 s.[17] Although Fang et al.[19] managed to reduce the texturing time to 100 ms; the process time presented in this study was 500 times shorter (200 µs). The reduced texturing time allows the creation of patterns with textures of diverse morphologies (e.g., circle, ellipsoid, square, and tangent cone), supporting commercial applications.

Textures with tangent cone shape exhibited a different cross-sectional profile in comparison with the other shaped textures because of the extreme elongation of the two-dimension morphology. Unlike findings by Kuang et al.,[11] the laser energy in this study was spatially distributed across the beam through the method presented. When LBS in two dimensions and is excessively large and narrow, the laser energy profile can be altered, as narrower regions lack sufficient area to support a Gaussian distribution. Consequently, the depth of the textures with tangent cone geometry was shallower within the regions with narrower shape, suggesting that the laser energy peaks require an adequate area to maintain the Gaussian profile. In contrast, the other textures had Gaussian profiles of the energy, their border provide sufficient space to sustain the laser energy peaks.

5. Conclusions

This investigation demonstrated the application of the LBS technology using an infrared (1064 nm) nanosecond pulsed (200 ns) laser beam and LC-SLM, along with a novel method to process 316 L surface with textures of varied shapes. The findings of this study demonstrate that: LBS can be effectively performed using infrared nanosecond pulsed laser using a novel, simplified method that combines GCH with PowerPoint. This technique enables the creation of laser beam at microscale with diverse geometries (i.e., cycler, triangle, pentagon, and tangent cone). The size of the laser beam on the target surface is defined solely by the area ratio of the geometry relative to background, contrasting with the findings of previous studies. The distance from LC-SLM to galvanometer mirror scanner focal lens and superimposed Fresnel focal length determine the image reconstruction length. Maximum unit cell size plays a critical role in determining the shaped laser-beam quality. The shaped textures with depths ranging from 6 to 12 µm, and width between 45 and 70 µm were achieved on 316 L using only 5 pulses, resulting in high-quality shape and a single texture production of 200 µs. The fast texture creation rate enables to texture of large areas (10 × 10 mm) in a short time period (2 s) with microtextures of substantial depth. Most LBS retain Gaussian profile of the laser energy spatial distribution. The laser beam shaped with tangent cone morphology, however, is an exception, exhibiting a "wedge" profile in energy spatial distribution.

This study demonstrates the applicability of the LBS on nanosecond pulsed laser using LC-SLM to texture 316 L with various geometries efficiently and over large surface areas. The ability of the design of the dimple shape provides opportunities to functionalize the surface for various applications, including improving the wear resistance, decreasing the coefficient of friction, antifouling application, enhancing corrosion resistance, adhesion properties, and other surface performance enhancements. This advantage addresses previously unmet needs, highlighting the potential of this technology for diverse industrial applications, such as automotive, aerospace, biomedical, energetic, and maritime.

In future works, the influence of the laser parameters, including pulse energy, pulse length, and pulse number, on the quality and dimension of the shaped dimples will also be investigated.

Conflict of Interest

The authors declare no conflict of interest.

Data Availability Statement

The data that support the findings of this study are available from the corresponding author upon reasonable request.

Keywords

laser-beam shaping, laser-surface texturing, liquid crystal-spatial light modulator, metallic alloys, nanosecond pulsed laser

Received: April 1, 2025
Revised: September 30, 2025
Published online:

[1] A. Al-Mahdy, J. I. Ahuir-Torres, T. T. Öpöz, H. R. Kotadia, J. Mullett, M. C. Sharp, *Opt. Laser Technol.* **2025**, *181*, 111626.
[2] B. Mao, A. Siddaiah, Y. Liao, P. L. Menezes, *J. Manuf. Process.* **2020**, *53*, 153.
[3] A. M. Mohamed, A. M. Abdullah, N. A. Younan, *Arab. J. Chem.* **2015**, *8*, 749.
[4] N. Sirdeshmukh, G. Dongre, *Mater. Today Proc.* **2021**, *44*, 2348.
[5] L. Vedaprakash, R. Dineshram, K. Ratnam, K. Lakshmi, K. Jayaraj, S. M. Babu, R. Venkatesan, A. Shanmugam, *Colloids Surf B Biointerfaces* **2013**, *106*, 1.
[6] H. Wang, G. P. Goodrich, F. Tam, C. Oubre, P. Nordlander, N. J. Halas, *J. Phy. Chem. B* **2005**, *109*, 11083.
[7] I. Etsion, *Recent Developments in Wear Prevention, Friction and Lubrication*, Research Signpost, India **2010**, 137.
[8] J. Wahab, M. Ghazali, W. Yusoff, Z. Sajuri, *Trans. IMF* **2016**, *94*, 193.
[9] V. Kumar, R. Verma, S. Kango, V. S. Sharma, *Mater. Today Commun.* **2021**, *26*, 101736.
[10] A. Nsilani Kouediatouka, Q. Ma, Q. Liu, F. J. Mawignon, F. Rafique, G. Dong, *Coatings* **2022**, *12*, 1015.
[11] Z. Kuang, J. Li, S. Edwardson, W. Perrie, D. Liu, G. Dearden, *Opt. Lasers Eng.* **2015**, *70*, 1.
[12] F. M. Dickey, S. C. Holswade, *Laser Beam Shaping Applications*, CRC Press, Taylor & Francis Group, USA **2017**, p. 383.
[13] Y.-D. Chen, W.-J. Tsai, S.-H. Liu, J.-B. Horng, *Appl. Surf. Sci.* **2015**, *353*, 568.
[14] F. M. Dickey, L. S. Weichman, R. N. Shagam, *High-Power Laser Ablation III*, Processing of SPIE, USA, SPIE pp. 338–48.
[15] G. Lazarev, A. Hermerschmidt, S. Krüger, S. Osten, *Opt. Imag. Metrolog. Adv. Technol.* **2012**, 1.
[16] R. J. Beck, J. P. Parry, W. N. MacPherson, A. Waddie, N. J. Weston, J. D. Shephard, D. P. Hand, *Optics express* **2010**, *18*, 17059.
[17] J. Li, Z. Kuang, S. Edwardson, W. Perrie, D. Liu, G. Dearden, *Appl. Opt.* **2016**, *55*, 1095.
[18] D. Liu, Y. Wang, Z. Zhai, Z. Fang, Q. Tao, W. Perrie, S. P. Edwarson, G. Dearden, *Opt. Laser Technol.* **2018**, *102*, 68.
[19] Z. Fang, T. Zhou, W. Perrie, M. Bilton, J. Schille, U. Löschner, S. Edwardson, G. Dearden, *Materials* **2022**, *15*, 9059.
[20] J. J. Kaakkunen, I. Vanttaja, P. Laakso *J. Laser Micro Nanoeng.* **2014**, *9*, 37.
[21] J. Dupuy, H. Von Horsten, M. Lamblin, Y. Hernandez, *J. Laser Micro Nanoeng.* **2020**, *15*, 228.
[22] K. L. Wlodarczyk, D. P. Hand, *Appl. Opt.* **2014**, *53*, 1759.
[23] A. Al-Mahdy, H. Kotadia, M. Sharp, T. Opoz, J. Mullett, J. Ahuir-Torres, *Lasers Manuf. Mater. Process.* **2023**, *10*, 141.
[24] J. Li, Y. Tang, Z. Kuang, J. Schille, U. Loeschner, W. Perrie, D. Liu, G. Dearden, S. Edwardson, *Opt. Lasers Eng* **2019**, *112*, 59.
[25] Z. Kuang, W. Perrie, D. Liu, S. P. Edwardson, Y. Jiang, E. Fearon, K. G. Watkins, G. Dearden, *Appl. Surface Sci.* **2013**, *273*, 101.
[26] T. Zhou, S. Kraft, W. Perrie, J. Schille, U. Löschner, S. Edwardson, G. Dearden, *Materials* **2021**, *14*, 2243.
[27] J. P. Parry, R. J. Beck, J. D. Shephard, D. P. Hand, *Appl. Opt.* **2011**, *50*, 1779.
[28] P. Kumar, N. K. Nishchal, *Opt. Lasers Eng* **2021**, *146*, 106720.
[29] J. Ahuir-Torres, M. Sharp, *Lasers Manuf. Mater. Process.* **2022**, *9*, 454.
[30] J. Terragni, A. Miotello, *Micromachines* **2021**, *12*, 300.
[31] M. V. Shugaev, M. He, Y. Levy, A. Mazzi, A. Miotello, N. M. Bulgakova, L. V. Zhigilei, *Handbook Of Laser Micro-And Nano-Engineering*, Springer, Germany **2021**, pp. 83–163.
[32] D. Flamm, D. G. Grossmann, M. Sailer, M. Kaiser, F. Zimmermann, K. Chen, M. Jenne, J. Kleiner, J. Hellstern, C. Tillkorn, *Opt. Eng.* **2021**, *60*, 025105.

